Postprint of: Shopa M., Ftomyn N.: Application of two-dimensional intensity maps in high-accuracy polarimetry, JOURNAL OF THE OPTICAL SOCIETY OF AMERICA A-OPTICS IMAGE SCIENCE AND VISION, Vol. 36, iss. 4 (2019), pp.485-491, DOI: 10.1364/JOSAA.36.000485

Application of 2D intensity maps in high accuracy polarimetry

MYKOLA SHOPA[1]*, NAZAR FTOMYN[2]

[1]*Department of Atomic, Molecular and Optical Physics, Faculty of Applied Physics and Mathematics, Gdańsk University of Technology, Narutowicza 11/12, 80-233 Gdańsk, Poland*
[2]*Ivan Franko National University of Lviv, 8 Kyrylo and Mefodiy St. 79005 Lviv, Ukraine*
* *mykola.shopa@pg.edu.pl*

Received XX Month XXXX; revised XX Month, XXXX; accepted XX Month XXXX; posted XX Month XXXX (Doc. ID XXXXX); published XX Month XXXX

We propose the analysis of the 2D intensity contours maps which is based on the optical transmission function for the polarizer-specimen-analyzer system. The small modification of HAUP technique (high-accuracy universal polarimeter) was used to measure the intensity maps (HAUP maps), determine the phase retardation, linear dichroism (LD) parameters and multiple light reflection contribution in uniaxial crystals. We have performed measurements in direction perpendicular to the optical axis on pure birefringent $LiNbO_3$, birefringent optically active SiO_2 and two birefringent optically active dichroic galogermanate crystals doped with Mn^{3+} and Cr^{3+} ions. We have obtained good agreement of the experimental data for 532, 633 and 650 nm wavelengths with analytical values. These results extend the capabilities of the high-accuracy polarimetry to the anisotropic crystal studies.

OCIS CODES: (120.5410) POLARIMETRY, (260.5430) POLARIZATION, (260.1180) CRYSTAL OPTICS, (260.1440) BIREFRINGENCE, (050.1930) DICHROISM

http://dx.doi.org/10.1364/AO.99.09999

1. INTRODUCTION

The high accuracy polarimetry is one of the most precise experimental methods in crystal optics studies. HAUP version, introduced in 1983 [1], has undergone multiple upgrades over time – in the form of the spectropolarimeter [2], enhanced HAUP for significantly anisotropic crystals with linear and circular dichroism [3–5], fast-type HAUP with CCD spectrometer [6], dual-wavelength polarimeter [7-9]. Despite the fact, that there are other experimental methods of solving crystal optics problems (for example, tilter-polarimeter [10,11] or Mueller matrix polarimeter [12–14]), HAUP still remains as one of the most popular methods.

The fundamental advantage of HAUP is its versatility, i.e. possibility of simultaneous measurement of main anisotropic optical properties of the crystal (linear birefringence (LB), circular birefringence, linear and circular dichroism), and parametric optical phenomena (electrooptic or electrogyration effect). The basic optical setup of polarizer-sample-analyzer (PSA) is used in HAUP and there is no need in additional elements to change polarization state of the light, like photoelastic modulators in [12], but the requirements for the quality of the optical elements are very high.

The peculiarity of HAUP is that the polarizer azimuth θ and analyzer azimuth χ, which are both measured from the principal crystal axes, are very small (they hardly reach 10^{-2} rad). It means, that the initial setup of the polarizers at different angular positions within these ranges must be very accurate. The transmitted light intensity is precisely measured as a function of the polarizer position θ and relative polarizer-analyzer angle $Y = \chi - \theta$.

In this paper we discuss the application examples of the 2D maps of the light intensity in the shape of ellipses, which, in high accuracy polarimetry, can be analyzed to determine the parameters related to the optical properties of the crystals. The definition „HAUP map" for the intensity contours of the bivariate transmission function was introduced by Moxon and Renshaw [4]. They considered theoretically the properties of the 2D intensity maps for different crystal anisotropy parameters and systematic errors of the polarimeter. Although, conventional HAUP has been used multiple times by different authors, HAUP maps were hardly ever used for experimental data processing. Only in experimental work [15], the preliminary results of linear dichroism (LD) calculations, using the HAUP map analysis, have been presented for one of the crystals from the langasite family.

In current paper, we have analytically and then experimentally considered several optical anisotropy parameters manifestations in the HAUP map. We have also considered the multiple light reflections (MLR) and LD superposition effect and the possibility of separation of the corresponding parameters. In order to eliminate the possible errors we have also used lasers with different wavelengths in the experimental setup. Experiments have been carried out in the perpendicular to the optical axis direction of uniaxial crystals using a modified HAUP technique. As samples we have used cut crystal plates with the optical axis always in the surface plane.

2. HAUP MAPS IN THE PSA SYSTEM

In the transparent optically active crystals two elliptically polarized eigen waves propagate with different velocities and with the opposite sign of ellipticity k. In general, two main refractive indices n_1 and n_2

correspond to the two eigen polarizations. They define the birefringence $\Delta n = n_2 - n_1$, and phase difference or retardation $\Gamma = \frac{2\pi}{\lambda}\Delta n z$, where λ is the wavelength of light and z is the specimen thickness.

In current study, the main attention was paid to the investigation of the 2D intensity maps which have been described in [4] for the first time. We have examined the 2D intensity maps in polarizer azimuth θ and analyzer azimuth χ coordinates. For small polarizers azimuths ($\theta, \chi \le 1^\circ$), the transmission function $J(\theta,\chi)$ of the PSA system can be written in a matrix form as [2,3]:

$$J(\theta,\chi) = \begin{bmatrix} 1 & (\chi-\theta) & (\chi-\theta)^2 \end{bmatrix} \mathbf{C} \begin{pmatrix} 1 \\ \theta \\ \theta^2 \end{pmatrix}. \qquad \textbf{(1)}$$

For optically active birefringent crystal, without taking second-order terms and parasitic ellipticity of the polarizer and analyzer [1,2,16,17] into account, the nonzero components of the matrix **C** are [2,3,18]: $C_{13} = 2(1-\cos\Gamma)$, $C_{21} = -2k\sin\Gamma$, $C_{22} = 2(1-\cos\Gamma)$, $C_{31} = 1$. Then from (1) we obtain the transmission function, that describes the second order surface in two variables (θ,χ) and contains, exclusively, θ^2, χ^2, $\theta\chi$, θ, χ terms. It has a form of an elliptic paraboloid, in general:

$$J(\theta,\chi) = a\theta^2 + 2b\theta\chi + c\chi^2 + 2d\theta + 2f\chi + g. \qquad \textbf{(2)}$$

According to equation (1) $a = c = 1$, $b = -\cos\Gamma$, $d = k\sin\Gamma$, $f = -k\sin\Gamma$ and $g = 0$. The transmitted intensity does not contain the isotropic term, conditioned by the absorption and the reflection of light.

Intersections of the $J(\theta,\chi)$ surface with planes of equal transmitted intensities $J(\theta,\chi) = J_0 = \text{const}$ have the shapes of ellipses. The full sets of these cross sections form the 2D intensity maps (HAUP maps) [2,15]. Experimentally, instead of $J(\theta,\chi)$, one measure some intensity value $I(\theta,\chi)$ in arbitrary units. However, by choosing the appropriate J_0 constant, we can get *a* and *c* coefficients next to θ^2 and χ^2 to be equal 1, as in equation (2). Therefore, the major axes of ellipses on the 2D maps are always tilted by 45° and the ratio of semi-major to semi-minor axes depends on the phase difference Γ.

3. MEASUREMENT OF THE 2D INTENSITY MAPS

Universal, related to HAUP, laser polarimeter, based on the PSA optical scheme and full computer control (Figure 1), has been used for the numerous important anisotropic materials studies [7-9, 19-21]. In our most recent version the high quality Glan-type calcite prisms with extinction ratio of 10^{-5} (specified by the manufacturer) and a clear aperture of 10×10 mm² have been used. Angular resolution (minimal rotation angle) of the polarizers was approximately 4×10^{-3} degree over the 20 degrees range. As light sources we have used He-Ne laser (λ = 633 nm), semiconductor red laser with wavelength of 650 nm and diode pumped solid state laser with λ = 532 nm.

The light transmitted through the PSA system has been detected with a photodiode followed by a high impedance operational amplifier and 24-bit analog-to-digital converter. The computer has controlled the reference light intensity prior to the beam entrance to the polarizer, the intensity of the light transmitted through the analyzer, the stepper motors orientations and the temperature of the sample.

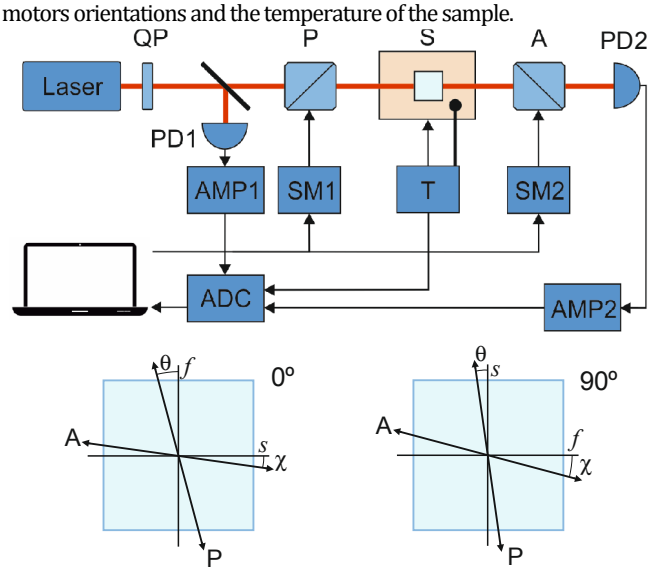

Fig. 1. Schematic representation of the experimental setup. L: laser; QP: quarter-wave plate; P: polarizer; S: sample; A: analyzer; PD1, PD2: photodetectors; AMP1, AMP2: high impedance amplifiers; SM1, SM2: stepper motors; T: temperature stabilizer; ADC: analog-to-digital converter. The two crystal sets (0º and 90º) in PSA system are also presented. *θ*: rotation angle of polarizer; *χ*: rotation angle of analyzer; f, s: fast and slow axis of the sample.

In HAUP setup we have measured the transmitted light intensity by scanning the grid of usually 21×21 points of θ_i and χ_j, with a step of approximately 0.05°. In our polarimetric method the scanning area is usually a parallelogram, which is defined by the phase difference Γ [9]. Dependencies of the absolute intensities $I_i(\chi)$ on a small angle of the analyzer rotation χ for all fixed θ_i azimuths are always parabolic:

$$I_i(\chi) = A_i\chi^2 + B_i\chi + C_i, \qquad \textbf{(3)}$$

where $\chi_{\min} = -B_i / 2A_i$. With A_i, B_i, C_i coefficients we can calculate the array $I(\theta_i,\chi_j)$ of the intensities values on the square grid and later find the values of these coefficients from (2). The analyzer azimuth $\chi_{\min}$, which corresponds to the minimum transmission of the PSA system, i.e. $\left(\frac{\partial I}{\partial\chi}\right)_\theta = 0$, depends on the polarizer azimuth θ as:

$$\chi_{\min}(\theta) = \theta\cos\Gamma + k\sin\Gamma. \qquad \textbf{(4)}$$

Consequently, the locus of the χ_{min} points in the (θ,χ) coordinate system is a straight line and the tangent of the slope angle of linear dependence (3) in PSA system is equal to $\left(\frac{\partial\chi_{\min}}{\partial\theta}\right)_{\text{PSA}} = \cos\Gamma$. Naturally, in the polarizer-analyzer (PA) system $\left(\frac{\partial\chi_{\min}}{\partial\theta}\right)_{\text{PA}} = 1$.

Two crystal sets have been used in the PSA system during the experiment: 0° when the plane of the incident light polarization was close to the fast crystal axis; 90° when the crystal was rotated by 90° around the beam direction and the incident light polarization was close to the slow crystal axis (see Figure 1). Rotation of the sample by 90°

around the incident light reverses the signs of Γ and k parameters [1,3,4].

4. HAUP MAPS FOR DICHROIC OPTICALLY ACTIVE CRYSTALS

In case of significant optical anisotropy of crystal (presence of the linear and circular birefringence, as well as linear and circular dichroism) nonzero components of the **C** matrix are [3,5,6]:

$$C_{11} = \text{const}\,, \qquad C_{12} = 4K\left(\cos\Gamma - \cosh E\right),$$
$$C_{13} = 2\left(\cosh E - \cos\Gamma\right),$$
$$C_{21} = 2K\left(\cos\Gamma - e^{E}\right) - \frac{2k}{E^2/\Gamma^2+1}\sin\Gamma\,,$$
$$C_{22} = 2\left(e^{E} - \cos\Gamma\right), \qquad C_{31} = e^{E}. \qquad \textbf{(5)}$$

Here $K = \left[k\left(E/\Gamma\right)+k'\right]/\left[\left(E/\Gamma\right)^2+1\right]$ is the superposition of the eigen waves ellipticity k, $E = \left(2\pi/\lambda\right)\Delta m z$ is the linear dichroism parameter, which depends on the difference between the principal extinction coefficients $\Delta m = m_z - m_y$ for two orthogonal linear polarization states, and $k' = \left(2\pi/\lambda\right)\Delta\kappa z$ is the parameter of the circular dichroism, which depends on the difference $\Delta\kappa = \kappa_l - \kappa_r$ between the extinction coefficients for left and right circularly polarized light.

By taking the new **C** matrix components into account and neglecting terms which are proportional to k^2, K^2 etc. for the transmitted intensity function (1) we obtain the elliptic paraboloid (2), with coefficients:

$$a = e^{-E}\,, \quad b = -2\cos\Gamma\,, \qquad c = e^{E}\,,$$
$$d = K\left(\cos\Gamma - e^{E}\right) + \frac{k}{E^2/\Gamma^2+1}\sin\Gamma\,,$$
$$f = K\left(\cos\Gamma - e^{E}\right) - \frac{k}{E^2/\Gamma^2+1}\sin\Gamma\,. \qquad \textbf{(6)}$$

For purely birefringent and optically active crystal, when $E = 0$ and $k' = 0$, these coefficients equal those already mentioned in [7]. It is important that coefficients a and c are not equal and depend only on the parameter of linear dichroism E. Unequal coefficients at θ^2 and χ^2 in equation (2) indicate that LD leads to the rotation of the major axes of ellipses on the 2D maps, with the angle of rotation dependent on the phase difference Γ and LD parameter E. It is obvious, that

$$\tan 2\xi = \frac{b}{a-c} = \frac{2\cos\Gamma}{e^{E}-e^{-E}}\,, \qquad \textbf{(7)}$$

where ξ is the counterclockwise angle of rotation of the major axis of the ellipse from the θ -axis. The tangent of the slope angle of the lines $\chi_{\min}(\theta)$ in dichroic crystals is equal to $\frac{\partial\chi_{\min}}{\partial\theta} = \frac{\cos\Gamma}{e^{E}}$. Accordingly, $\frac{\partial\chi_{\min}}{\partial\theta}$ value, which can be easily measured experimentally, is not always equal to $\cos\Gamma$, as in equation (3), but contains also information about LD. However, the 2D maps give chance to determine the ellipse's rotations angle ξ and then by relations

$$\cos\Gamma = \frac{\partial\chi_{\min}}{\partial\theta}\sqrt{\frac{\tan 2\xi}{\tan 2\xi - 2\partial\chi_{\min}/\partial\theta}}\,,$$
$$E = \frac{1}{2}\ln\left(\frac{\tan 2\xi}{\tan 2\xi - 2\partial\chi_{\min}/\partial\theta}\right), \qquad \textbf{(8)}$$

calculate the correct values of $\cos\Gamma$ and parameter E of the LD in dichroic crystals. In addition to the alternating sign of the Γ and k parameters, rotation of the sample by 90° around the incident beam also reverses the signs of E and ξ.

In experiment it is important that Γ, E and k' values depend on the thickness of the sample z, and at the same time eigen waves ellipticity k does not depend on z. We should note, that one can use the approximation $e^{E} \approx 1 + E$, when $E \ll 1$, which can be achieved by the sample thickness reduction.

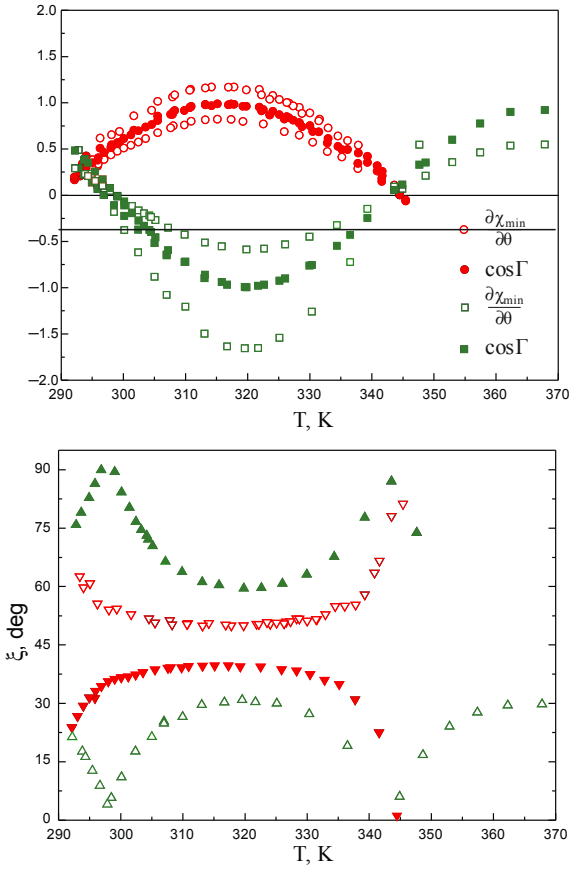

Fig. 2. Acquired measurement results on a SGG: Mn^{3+} crystal plate, 1.51 mm thick. The various experimental points correspond to 0º (open symbols) and 90º (solid symbols) crystal sets as well as two different wavelengths. Upper panel: measured $\frac{\partial\chi_{\min}}{\partial\theta}$ (○, □) and calculated $\cos\Gamma$ (●, ■) values for λ = 532 nm (□, ■) and λ = 650 nm (○, ●). Lower panel: angle of rotation ξ of the major axis of the ellipse on the HAUP maps from the θ -axis for λ = 532 nm (△, ▲) and λ = 650 nm (▽, ▼).

Using these properties of the HAUP maps in the (θ,χ) coordinate system, we have measured the value of LD in langasite family $Sr_3Ga_2Ge_4O_{14}$ (SGG) single crystal, doped with Mn^{3+} ions (0.1 at %). Figure 2 presents the temperature dependence of the corresponding anisotropy parameters for two wavelengths (532 and 650 nm) and two (0° and 90°) crystal sets (open and solid symbols).

It is important to note the considerable difference between the extremum values of $\frac{\partial\chi_{\min}}{\partial\theta}$ and $\cos\Gamma$ caused by LD, and, respectively, significant rotations of the ellipses on the HAUP maps relative to the value of 45º for non-dichroic crystals. For two sample sets in PSA system (0º and 90º) the angles ξ of these rotations differ from 45° only by sign (lower panel in Figure 2) and the differences $45°-\xi$ are the most significant when $\frac{\partial\chi_{\min}}{\partial\theta}\to 0$. We note here that at this temperature the ellipses on the 2D maps become circles and the rotation angles are meaningless. The actual $\cos\Gamma$ values (upper panel in Figure 2), calculated using formulas (8), do not depend on the crystal set.

The LD parameters E have opposite signs for two (0º and 90º) crystal sets, but their absolute values are very close to each other (Figure 3). At the wavelength of 532 nm the difference between the extinction coefficients is $\Delta m\approx 3.0\times10^{-5}$ and at wavelength of 650 nm – $\Delta m\approx 1.2\times10^{-5}$. The described polarimetric method of the LD measurement complement the traditional two-spectra and differential methods for anisotropic samples [22] and allows steadfast measurement of the Δm value, which is significantly smaller than 5.0×10^{-6}.

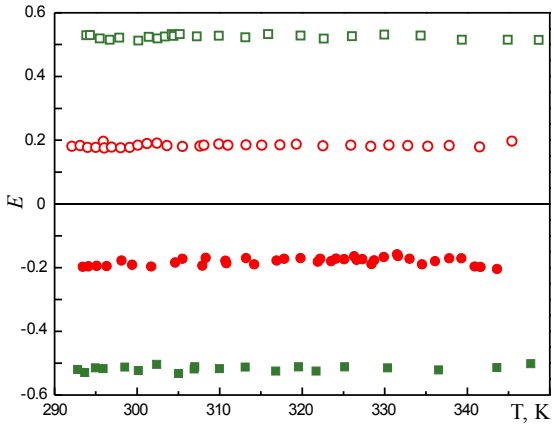

Fig. 3. The temperature dependencies of the LD parameter E in Mn-doped SGG crystal for λ = 532 nm (□, ■) and λ = 650 nm (○, ●) for two (0º and 90º) crystal sets (open symbols, solid symbols).

5. MULTIPLE LIGHT REFLECTIONS MANIFESTATION IN HAUP MAPS

5.1. Expression for the transmitted intensity

The effect of multiple light reflections (MLR) is often observed in polarimetric experiments with crystal samples with high surface parallelism. The authors of several works have reported in their results the influence of MLR in the high accuracy polarimetry. Principally, this effect is manifested in the form of oscillations in temperature dependencies of the phase difference Γ and, consequently, other parameters, that depend on the Γ. For example, a lithium niobate ($LiNbO_3$) was sometimes used as the reference crystal, since it is optically inactive (eigen waves ellipticity $k=0$) [15, 23-25] and makes it possible to find the systematic errors easily. However, good sample quality and relatively high refractive index are always the cause of the MLR effect. It is interesting to note here, that influence of the imperfect parallelism of crystal faces on high-accuracy universal polarimeter measurements is also considered in [26].

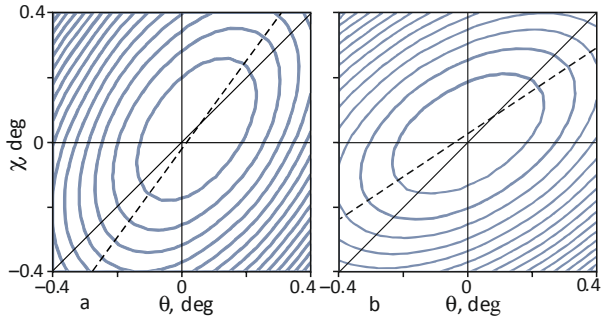

Fig. 4. Equi-intensity contours on the two HAUP maps measured for λ = 633 nm at different temperatures on $LiNbO_3$ crystal show the influence of MLR. The dashed lines are parallel to the major axes of ellipses.

In Figure 4 we present the examples of two maps, that have been measured with $LiNbO_3$ crystal and which show how MLR affects the experimental results. One can easily see the rotation of the major axis of the ellipse on the 2D maps with regarding to the line $\chi=\theta$, measured beforehand in PA system. These rotations, calculated from the first part of equation (7), are equal to $\xi_a=53.8°$ and $\xi_b=33.6°$ for *a* and *b* cases respectively, i.e. they have different rotation directions when compared to the 45° line. Let us notice, that eccentricities of the ellipses in Figure 4a,b are the same, therefore, phase differences Γ should be comparable at these temperatures. But measured values of $\frac{\partial\chi_{\min}}{\partial\theta}$ in Figure 4 are different and are equal to $\left(\frac{\partial\chi_{\min}}{\partial\theta}\right)_a=0.568$ and $\left(\frac{\partial\chi_{\min}}{\partial\theta}\right)_b=0.387$ respectively. Since the MLR is also manifested as dichroism, i.e. in the ellipse rotations on the HAUP maps, the authors of [16] introduced an effective linear dichroism of $LiNbO_3$ to include this phenomenon.

To find the actual value of $\cos\Gamma$, we have to find the transmitted intensity of the PSA system and take the MLR into account (see Appendix).

With accuracy to isotropic multiplier, which contains isotropic absorption parameters, and neglecting higher order terms, we acquire formula for transmission function:

$$J(\theta,\chi)=\frac{e^{-E}}{B}\theta^2+\frac{e^{E}}{A}\chi^2-$$
$$-\frac{2}{AB}\left[\cos\Gamma-2r_0^2e^{-\alpha z}\left(2\cos^2\frac{\Gamma}{2}\sinh E+2\cos^2\varphi\cosh E-e^{E}\right)\right]\theta\chi+$$
$$+F_1\theta+F_2\chi+\text{const}, \qquad (9)$$

where $\varphi=(2\pi/\lambda)\bar{n}z$ is the average phase change for two eigen modes inside the crystal, α is the absorption coefficient, $r_0^2=(\bar{n}-1)^2/(\bar{n}+1)^2$, $A=1-2r_0^2e^{E-\alpha z}\cos(2\varphi+\Gamma)$, $B=1-2r_0^2e^{-E-\alpha z}\cos(2\varphi-\Gamma)$ and $\bar{n}$ is the mean refractive index.

The functions F_1 and F_2, that are included in relation (9), are very cumbersome and they do not affect the ellipses rotations in the 2D maps, so we do not present their expressions.

The relations for the tangent of the slope angle $\frac{\partial\chi_{\min}}{\partial\theta}$ of lines $\chi_{min}(\theta)$ in PSA system and for angle ξ of ellipses rotations are the following:

$$\frac{\partial\chi_{\min}}{\partial\theta}=\frac{\cos\Gamma-2r_0^2e^{-\alpha z}\left(2\cos^2\frac{\Gamma}{2}\sinh E+2\cos^2\varphi\cosh E-e^E\right)}{\mathrm{e}^E-2r_0^2e^{-\alpha z}\cos 2\varphi\cos\Gamma-2r_0^2e^{-\alpha z}\sin 2\varphi\sin\Gamma} \quad \textbf{(10)}$$

$$\tan 2\xi=-\frac{\cos\Gamma-2r_0^2e^{-\alpha z}\left(2\cos^2\frac{\Gamma}{2}\sinh E+2\cos^2\varphi\cosh E-e^E\right)}{\sinh E-2r_0^2e^{-\alpha z}\sin 2\varphi\sin\Gamma}. \quad \textbf{(11)}$$

We shall consider two application examples of these equations in analyzing the 2D maps and calculation of the phase difference Γ.

5.2. Multiple light reflections in non-dichroic quartz crystal

We have observed the MLR effect in high-quality quartz plate, $z=2.113$ mm thick. At room temperature it is a half-wave plate ($\cos\Gamma=-1$) for wavelength $\lambda=633$ nm. Since quartz crystal does not have LD for this wavelength and it can be considered transparent for He-Ne laser light, we can introduce some simplifications into equations (10,11):

$$\frac{\partial\chi_{\min}}{\partial\theta}=\frac{\cos\Gamma-2r_0^2\cos 2\varphi}{1-2r_0^2\cos 2\varphi\cos\Gamma-2r_0^2\sin 2\varphi\sin\Gamma}. \quad \textbf{(12)}$$

$$\tan 2\xi=-\frac{\cos\Gamma-2r_0^2\cos 2\varphi}{2r_0^2\sin 2\varphi\sin\Gamma}. \quad \textbf{(13)}$$

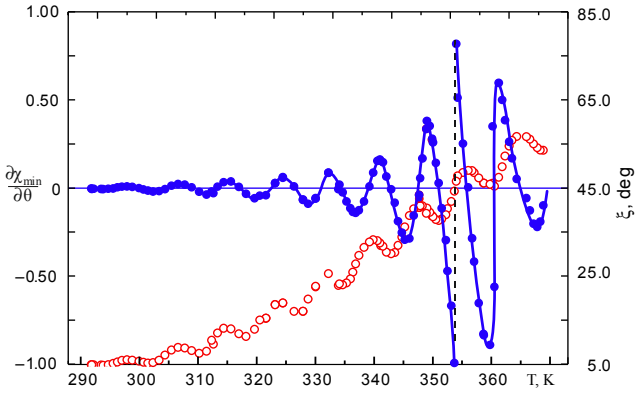

Fig. 5. Temperature dependencies of $\frac{\partial\chi_{\min}}{\partial\theta}$ (○) and rotation angle ξ of equi-intensity ellipses (●), acquired by the analysis of the HAUP maps and wavelength $\lambda=633$ nm on a high-quality SiO_2 plate.

Figure 5 presents measured temperature dependence of $\frac{\partial\chi_{\min}}{\partial\theta}$, which in absence of MLR should be equal to $\cos\Gamma$. MLR is the reason of oscillations, which are clearly visible in temperature dependence of $\frac{\partial\chi_{\min}}{\partial\theta}$. Maximum amplitude of these oscillations is at the temperature region, where $\cos\Gamma\approx 0$ and gradually decreases when temperature approaches values at which $\cos\Gamma\approx\pm 1$. This result correlates with equation (12).

Using the HAUP maps analysis, rotations of equi-intensity ellipses for each temperature have been calculated using equation (7). At phase difference $\Gamma=\frac{\pi}{2}+2m\pi$ (m – integer) angles ξ become abnormally high (Figure 5). At the same time, maximum deviations in determination of $\cos\Gamma$ remain almost constant. It can be explained by the fact, that ellipses eccentricities on the HAUP maps approach zero and even high-angle rotations do not affect the measurement of $\chi_{\min}(\theta)$ significantly.

System of equations (12,13) is nonlinear, therefore it is convenient to solve it using numerical methods, assuming that parameter r_0^2 stays constant with the sample temperature change (refraction indices of quartz at $\lambda=632.8$ nm $n_o=1.5426$, $n_e=1.5517$ [27], and respectively $r_0^2=0.0461$). Temperature dependence of $\cos\Gamma$, acquired from equations (12,13), is shown in Figure 6a. Figure 6b displays $\cos 2\varphi$ temperature dependence (experimental data and approximation result) which has major contribution to the characteristic oscillations, seen in Figure 5, which have been measured directly during the experiment.

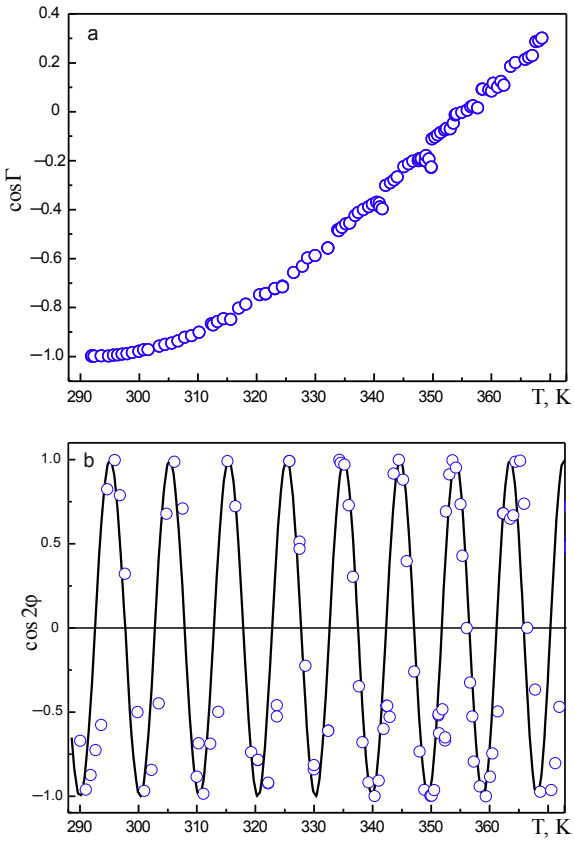

Fig. 6. Temperature dependencies of calculated $\cos\Gamma$ (a) and $\cos 2\varphi$ (b) on commercial plates of SiO_2 crystal. Solid line – result of approximation.

Therefore, the 2D maps analysis can serve as a criterion of accuracy of measurement of the crystal optics parameters. If the deviation from 45° of the slope angle of the ellipses major axes is noticeable on the

HAUP maps, then it is advisable to take MLR effects into account or take measures to limit its contribution.

5.3. Manifestation of the multiple light reflections in dichroic crystal

Let us consider equations (10,11) for the case, when LD cannot be neglected. We assume, that LD parameter E is small, that we can use the approximation $e^{E} \approx 1+E$. We can also neglect terms proportional to Er_0^2. Next, let us add the effective LD parameter $\tilde{E}$ in the case of MLR presence:

$$\frac{\partial\chi_{\min}/\partial\theta}{\tan 2\xi - \partial\chi/\partial\theta} = \frac{E - 2r_0^2 e^{-\alpha z}\sin 2\varphi\sin\Gamma}{1 - 2r_0^2 e^{-\alpha z}\cos 2\varphi\cos\Gamma} \approx \\ \approx E - 2r_0^2 e^{-\alpha z}\sin 2\varphi\sin\Gamma = \tilde{E} \qquad (14)$$

Experimentally measured temperature dependencies of $\tilde{E}$ for two crystal sets in the PSA system of Cr^{3+} doped Ca-galogermanate ($Ca_3Ga_2GeO_4O_{14}$) crystal with thickness of 0.72 mm are shown in Figure 7. Some oscillation of the effective $\tilde{E}$ parameter are linked to, according to (14), with MLR. In the temperature region of 290–350 K for $\lambda = 633$ nm the average value of $\tilde{E} \approx 0.13$ and the absorption coefficients difference ($\Delta m \approx 1.8\times10^{-5}$) is 10^3 times smaller than the one acquired in [5] for the dichroic crystal.

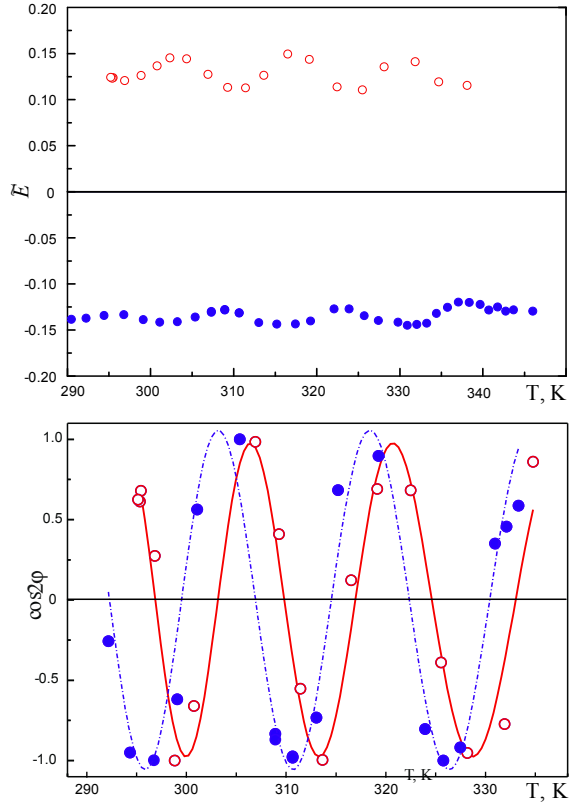

Fig. 7. Temperature dependencies of the effective parameter $\tilde{E}$ of LD and $\cos 2\varphi$ for two crystal sets (○ and ● refer to the 0° and 90° orientation of the plate in PSA system) of Cr^{3+} doped $Ca_3Ga_2GeO_4O_{14}$ crystal.

For the wavelength of He-Ne laser, using data [28], we get the values $2r_0^2 \approx 0.17$ and $e^{-\alpha z} \approx 0.59$ [29]. Since we have polished the crystals on our own, we can replace r_0^2 with βr_0^2, by introducing the empirical parameter β, which describes the sample imperfections (non-parallel facets, small light scattering) [30]. In our case, amplitudes of oscillations in Figure 7 for two crystal sets are different, therefore we should choose different values for β, in particular $\beta_0 = 0.2$ and $\beta_{90} = 0.1$. Unlike with the quartz crystal (section 5.2), where parameter $\beta = 1$, there are no visible oscillations in temperature dependencies of $\partial\chi_{\min}/\partial\theta$ and one can assume that $\cos\Gamma \approx \partial\chi_{\min}/\partial\theta$.

6. CONCLUSIONS

We have considered examples of direct applications of the 2D intensity maps in experimental results analysis in high accuracy polarimetry and improvement of the crystals optical anisotropy parameters measurement capabilities. We have not mentioned optical activity measurement results in this paper, because they have been discussed already in our previous articles. The influence of multiple light reflection in the high quality crystal plates on the polarimetric experiment has been measured and interpreted using the HAUP maps. These results are in reasonable agreement with previously reported for similar experiments [16, 31, 32] but without application of the 2D intensity maps. We have also established that multiple light reflection and linear dichroism are accompanied by rotations of the ellipse on the 2D maps so that the slope angle of the major axis differs from 45° value relative to the polarizer azimuth axis. It makes possible to easily determine the parameters of the linear dichroism and allows the detection of the difference between the absorption coefficients $\Delta m < 10^{-5}$ for two orthogonal eigen polarizations. Summarizing, we have extended the experimental measuring possibilities of the small quantities of linear dichroism in crystals.

APPENDIX: JONES MATRIX FOR ANISOTROPIC CRYSTAL WITH MULTIPLE LIGHT REFLECTIONS

For anisotropic crystal with MLR effect the Jones matrix $\tilde{\mathbf{M}}$ has been proposed in [16, 31, 32]. One of the possible ways of finding that matrix is presented in [31] and is the following:

$$\tilde{\mathbf{M}} = \mathbf{t}'\times\mathbf{S}\times\mathbf{M}\times\mathbf{t}, \qquad \mathbf{S} = (\mathbf{I}-\mathbf{N})^{-1}, \\ \mathbf{N} = \mathbf{M}\times\mathbf{\Omega}\times\mathbf{M}\times\mathbf{\Omega},$$

where $\mathbf{t}\times\mathbf{t}' = t^2\mathbf{I}$, $\mathbf{I}$ is the unit matrix, $\mathbf{M}$ is the Jones matrix for a single pass of light, given by [5] and multiplied by isotropic phase factor $\exp(i\varphi - \alpha z/2)$, $\mathbf{\Omega} = r_0\begin{pmatrix}1 & 0\\ 0 & -1\end{pmatrix}$ is the reflection matrix (see also comment from [33]). Then we have the following matrix

$$\tilde{\mathbf{M}} = t^2 e^{-\alpha z/2}\begin{pmatrix}\tilde{M}_{11} & \tilde{M}_{12}\\ \tilde{M}_{21} & \tilde{M}_{22}\end{pmatrix},$$

which elements are:

$$\tilde{M}_{11} = \frac{e^{i\left(\varphi+\frac{\Gamma}{2}\right)+\frac{E}{2}}}{1 - r_0^2 e^{i(2\varphi+\Gamma)+E-\alpha z}},$$

$$\tilde{M}_{12} = -\frac{2e^{i\varphi}(k'-ik)\sinh\frac{E+i\Gamma}{2}}{S'}\left[1 - r_0^2 e^{i2\varphi-\alpha z}\right],$$

$$\tilde{M}_{21} = \frac{2e^{i\varphi}\left(k' - ik\right)\sinh\frac{E+i\Gamma}{2}}{S'}\left[1 - r_0^2 e^{i2\varphi-\alpha z}\right],$$

$$\tilde{M}_{22} = \frac{e^{i\left(\varphi-\frac{\Gamma}{2}\right)-\frac{E}{2}}}{1 - r_0^2 e^{i(2\varphi-\Gamma)-E-\alpha z}},$$

and

$$S' = \left[1 - r_0^2 e^{i(2\varphi+\Gamma)+E-\alpha z}\right]\left[1 - r_0^2 e^{i(2\varphi-\Gamma)-E-\alpha z}\right].$$

The transmitted through the PSA system light intensity can be written as $J(\theta,\chi) = \left|\mathbf{A}^{+}\tilde{\mathbf{M}}\,\mathbf{P}\right|^2$, where $\mathbf{P}$ and $\mathbf{A}$ are the Jones vectors of polarizer and analyzer.

References

1. J. Kobayashi and Y. Uesu, "A new optical method and apparatus HAUP for measuring simultaneously optical activity and birefringence of crystals. I. Principles and construction", J. Appl. Crystallogr. 16, 204–211 (1983).
2. J. Moxon, A. Renshaw, I. Tebbutt, "The simultaneous measurement of optical activity and circular dichroism in birefringent linearly dichroic crystal sections: II. Description of apparatus and results for quartz, nickel sulphate hexahydrate and benzil", J. Phys. D: Appl. Phys. 24, 1187–1192 (1991).
3. E. Dijkstra, H. Meekes and M. Kremers, "The high-accuracy universal polarimeter", J. Phys. D: Appl. Phys. 24, 1861–1868 (1991).
4. J. Moxon and A. Renshaw, "The simultaneous measurement of optical activity and circular dichroism in birefringent linearly dichroic crystal sections. I. Introduction and description of the method", J. Phys.: Condens. Matter. 2, 6807–6836 (1990).
5. J. Kobayashi, T. Asahi, M. Sakurai, M. Takahashi, and K. Okubo, "Optical properties of superconducting $Bi_2Sr_2CaCu_2O_8$" Phys. Rev. B. 53, 11784–11795 (1996).
6. A. Takanabe, H. Koshima, T. Asahi, "Fast-type high-accuracy universal polarimeter using charge-coupled device spectrometer" AIP Advances. 7, 025209 (2017).
7. Y. Shopa, M. Shopa, N. Ftomyn, "Dual-wavelength laser polarimeter and its performance capabilities", Opto-Electron. Rev. 25, 6–9 (2017).
8. M. Shopa, N. Ftomyn, "Investigations of the optical activity of nonlinear crystals by means of dual-wavelength polarimeter", Opt. Eng. 57(3), 034101 (2018).
9. M. Shopa, N. Ftomyn, and Y. Shopa, "Dual-wavelength polarimeter application in investigations of the optical activity of a langasite crystal", J. Opt. Soc. Am. A 34, 943–948 (2017).
10. D. Mucha, K. Stadnicka, W. Kaminsky, and A.M. Glazer, "Determination of optical rotation in monoclinic crystals of tartaric acid, (2R,3R)-(+)-$C_4H_6O_6$, using the 'tilter' method" J. Phys.: Condens. Matter. 9, 10829–10842 (1997).
11. W. Kaminsky, "Experimental and phenomenological aspects of circular birefringence and related properties in transparent crystals" Rep. Prog. Phys. 63, 1575–1640 (2000).
12. O. Arteaga, A. Canillas, and G. E. Jellison, "Determination of the components of the gyration tensor of quartz by oblique incidence transmission two-modulator generalized ellipsometry," Appl. Opt. 48, 5307–5317 (2009).
13. O. Arteaga, J. Freudenthal and B. Kahr, "Reckoning electromagnetic principles with polarimetric measurements of anisotropic optically active crystals," J. Appl. Cryst. 45, 279–291 (2012).
14. S. Nichols, A. Martin, J. Choi, B. Kahr, "Gyration and permittivity of ethylenediammonium sulfate crystals" Chirality, 28, 460–465 (2016).
15. Y. Shopa, N. Ftomyn, "Polarimetric studies of linear dichroism in Cr-doped gallogermanate crystals", Ukr. J. Phys. Opt. 7, 183–188 (2006).
16. C.L. Folcia, J. Ortega, and J. Etxebarria, "Study of the systematic errors in the HAUP measurements", J. Phys. D: Appl. Phys. 32, 2266–2277 (1999).
17. C. Hernández-Rodríguez, P. Gomez-Garrido, and S. Veintemillas, "Systematic errors in the high-accuracy universal polarimeter: application to the determining temperature-dependent optical anisotropy of KDC and KDP crystals", J. Appl. Cryst. 33, 938–946 (2000).
18. M. Kremers, and H. Meekes, "The interpretation of HAUP measurements: a study of the systematic errors" J. Phys. D: Appl. Phys. 28 1195–1211 (1995).
19. Y. Shopa, L. Lutsiv-Shumskii, R. Serkiz, "Optical activity of the KDP group crystals" Ferroelectrics, 317, 79–82 (2005).
20. O. Vlokh, Y. Shopa, M. Kravchuk, "Measurements of optical activity in $Gd_2(MoO_4)_3$", Ferroelectrics, 203, 107–111 (1997).
21. Y. Shopa, N. Ftomyn, "Optical activity of $Ca_3Ga_2Ge_4O_{14}$ crystals: experiment and calculus", Optica Applicata. 43, 217–228. (2013).
22. A. Rodger, B. Nordén, "Circular Dichroism and Linear Dichroism", Oxford University Press, 1997. – 150.
23. J. Kobayashi, T. Asahi, S. Takahashi, A.M. Glazer, "Evaluation of the systematic errors of polarimetric measurements: application to measurements of the gyration tensors of α-quartz by the HAUP", J. Appl. Cryst. 21, 479–484 (1988).
24. C. Hernández-Rodríguez, P. Gomez-Garrido, and S. Veintemillas, "Systematic errors in the high-accuracy universal polarimeter: application to the determining temperature-dependent optical anisotropy of KDC and KDP crystals", J. Appl. Cryst. 33, 938–946 (2000).
25. J. Kobayashi, T. Asahi, M. Sakurai, I. Kagomiya, H. Asai and H. Asami, "The optical activity of lysozyme crystals", Acta Cryst. A54, 581–590 (1998).
26. J. Herreros-Cedrés, C. Hernández-Rodríguez, and R. Guerrero-Lemus, "Influence of the imperfect parallelism of crystal faces on high-accuracy universal polarimeter measurements", J. Opt. A: Pure Appl. Opt. 8, 44–48 (2006).
27. G. Ghosh, "Dispersion-equation coefficients for the refractive index and birefringence of calcite and quartz crystals", Opt. Commun. 163, 95-102 (1999).
28. K. Kaldybayev, A. Konstantinova, Z. Perekalina, Gyrotropy of uniaxial absorbing crystals (ISPIN, Moscow. 2000) (in Russian).
29. Y. Shopa, N. Ftomyn, "Linear dichroism spectra of doped calcium gallogermanate crystals", Acta Phys. Pol. A. 117, 114–116 (2010).
30. O. Kushnir, "Multiple reflections in crystals: natural and faraday optical activity", Ukr. J. Phys. Opt. 5, 87–95 (2004).
31. C. Hernández-Rodríguez, P. Gomez-Garrido, "Optical anisotropy of quartz in the presence of temperature-dependent multiple reflections using a high-accuracy universal polarimeter," J. Phys. D: Appl. Phys. 33, 2985–2994 (2000).
32. J. Simon, J. Weber, and H-G. Unruh, "Some new aspects about the elimination of systematical errors in HAUP measurements" J. Phys. D: Appl. Phys. 30, 676–682 (1997).
33. J. Herreros-Cedrés, C. Hernández-Rodríguez and R. Guerrero-Lemus, "Comment on 'Effect of multiple reflections of light on the optical characteristics of crystals'" J. Opt. A: Pure Appl. Opt. 7, 154–155 (2005).